

Band Calculation for Ce-compounds on the basis of Dynamical Mean Field Theory

Osamu SAKAI*, Yukihiko SHIMIZU¹ and Yasunori KANETA²

Department of Physics, Tokyo Metropolitan University, Hachioji 192-0397, Japan

¹*Department of Applied Physics, Tohoku University, Sendai 980-8579, Japan*

²*Department of Quantum Engineering and System Science, The University of Tokyo, Tokyo 153-8904, Japan*

(Received January 31, 2005)

The band calculation scheme for f electron compounds is developed on the basis of the dynamical mean field theory (DMFT) and the LMTO method. The auxiliary impurity problem is solved by a method named as NCA f^2v' , which includes the correct exchange process of the $f^1 \rightarrow f^2$ virtual excitation as the vertex correction to the non-crossing approximation (NCA) for the $f^1 \rightarrow f^0$ fluctuation. This method leads to the correct magnitude of the Kondo temperature, T_K , and makes it possible to carry out quantitative DMFT calculation including the crystalline field (CF) and the spin-orbit (SO) splitting of the self-energy. The magnetic excitation spectra are also calculated to estimate T_K . It is applied to Ce metal and CeSb at $T = 300$ K as the first step. In Ce metal, the hybridization intensity (HI) just below the Fermi energy is reduced in the DMFT band. The photo-emission spectra (PES) have a conspicuous SO side peak, similar to that of experiments. T_K is estimated to be lower than the CF splitting in γ -Ce, while to be higher in α -Ce. In CeSb, the double peak structure of PES is reproduced. In addition, higher T_K is obtained because HI is enhanced just at the Fermi energy in the DMFT band.

KEYWORDS: dynamical mean field theory, band theory, Ce metal, Ce-pnictides

1. Introduction

The non-empirical band calculation on the basis of the local density approximation (LDA) theory is one of the fundamental approaches to obtain the insight into the electronic properties of solid state materials. However, it has limitations to treat the dynamical excitation spectra (DES) of strongly correlated electron systems¹ such as f electron compounds. The understanding of DES of strongly correlated electrons has been extensively improved recently based on the approach of the dynamical mean field theory (DMFT).^{2,3} It seems natural to develop a non-empirical band calculation scheme for actual materials by the combination of LDA and DMFT.⁴⁻⁶

In the DMFT, the strongly correlated band electron problem is mapped onto the calcu-

*E-mail: sakai@phys.metro-u.ac.jp.

lation of DES of the auxiliary impurity Anderson model in an effective medium.³ At present, however, we do not have the theoretical method which analytically gives correct DES of the impurity Anderson model. Several numerical methods have been developed to calculate DES of the Kondo problem. It is known that the quantum Monte Carlo (QMC) method^{7,8} and the numerical renormalization group (NRG) method⁹ give in principle correct DES. They are applied to DMFT calculation,^{8,10} but they have difficulties in application to the realistic band calculation of *f* electron systems.^{6,11}

Approximate but highly flexible approaches have been developed on the basis of the resolvent technique.¹² The NCA method^{13,14} has been widely applied to various models though it has some weakness in application at very low temperatures: it does not fulfill the Fermi liquid relation. But it can be easily applied to realistic situations such as the competition between the Kondo effect and the crystalline field (CF) splitting.¹⁴ NCA has been also applied to the DMFT calculation.¹⁵ The NCA equation is justified by the $1/N_f$ expansion when the fluctuation of the valence is restricted to the f^1 and f^0 configurations, where N_f is the degeneracy factor of the *f* orbital.¹⁴ However, the exchange coupling through the virtual excitation to the f^2 configuration is not negligible in quantitative calculation. A scheme which includes the f^2 configuration in the frame work of the NCA type diagram has been used. However, it does not lead to the Kondo temperature (T_K) given by using the exchange constant obtained by the Schrieffer-Wolff (S-W) transformation.¹⁶ Therefore, the exchange process through the f^2 configuration is not properly accounted in the scheme. Actually, the DMFT calculation by using this method gives a too small Kondo resonance peak compared with the result using QMC method.⁶ In the DMFT band calculation, it is desirable to use a method which gives the correct order of magnitude of T_K .

A method to include the f^2 configuration within the $1/N_f$ order has been developed.^{17,18} The NCA equation is modified by a vertex correction term which leads to exchange coupling through the f^2 configuration. The self-consistency equation of this method needs huge computational time, if one tries to solve it strictly. But we can usually apply simplifying approximations for the equation.¹⁷ It does not need so much computational time, only few times larger than that of the NCA calculation, and gives T_K consistent with the result of the S-W transformation. We call the method as NCA f^2v' , henceforth, and is explained in Appendix.

Several efficient band calculation techniques have been developed.¹⁹ Among them the LMTO method is a very convenient one because it has formal similarity to the usual LCAO picture.²⁰ It is widely used though accuracy is not so very high when it is compared with other sophisticated methods. In this paper we develop a DMFT band calculation scheme by the combination of NCA f^2v' and LMTO methods, and apply it to Ce metal and CeSb as the first step.

The effective hybridization intensity (HI) is defined nominally as the product of the square

of the hybridization matrix and the density of states of conduction bands in the auxiliary impurity problem. It plays the key roles in the DMFT calculation. We mainly study how HI is modified in the DMFT calculation from that of LDA theory, and how the effects of the spin-orbit (SO) splitting and the CF splitting appear.

The relative occupation number of SO levels is strongly reduced from that of LDA in the correlated bands even when the total occupation number of the $4f$ electron is fixed near the value of LDA result.

Ce metal is known to have iso-structural *fcc* phases.²¹ The low temperature state is called as the α phase and it has smaller lattice constant. The higher temperature one is called as the γ phase. The DMFT studies on this transition have been extensively carried out.^{6,15,22,23} In these studies the SO and the CF splittings were neglected. In the present study we are not concerned with the $\alpha - \gamma$ transition, but we calculate the photo-emission spectra (PES)²⁴⁻²⁷ for the *fcc* state with the lattice constant of these two cases. The HI estimated by the LDA band has a peak just below E_F . This peak is reduced in the DMFT band, thus the SO side peak in PES becomes relatively conspicuous.

The CF level splitting is small in the auxiliary impurity model of γ -Ce, but the $\Gamma_7 \rightarrow \Gamma_8$ transition energy in the magnetic excitation is not small as the difference of HI also causes the CF energy difference. T_K in the Γ_7 is smaller than the CF excitation energy in γ -Ce. In α -Ce, T_K becomes larger than the CF excitation energy.

CeSb would be a first material for which HI calculated by the realistic band is used in the analysis of PES.^{25,28,29} The hybridization matrix is not small in the valence band region of Sb *p* states. In the energy region near E_F the density of states of bands is small reflecting the semi-metallic nature of the band structures. Various anomalous properties such as the very large magnetic anisotropy and the origin of the ferromagnetic layers in the ordered state are explained on the basis of the *p* - *f* mixing model proposed by Kasuya *et. al.*³⁰⁻³³ The top of the valence *p* band has the ($j = 3/2$) Γ_8 symmetry. A part of Γ_8 bands which has the same symmetry with that of the occupied *4f* band is pushed up above E_F due to the *p* - *f* hybridization in the ordered phase, and this plays important roles in the *p* - *f* mixing model. Such re-constructed electronic band structures in the ordered states are confirmed by the dHvA and the optical experiments.³⁴⁻³⁶ In the ordered states we can use the Hatree-Fock like static mean field approaches, and detailed comparison with experiments has been carried out.^{33,37} However, in the paramagnetic phase we need DMFT band calculation.

CeSb has a characteristic double peak structure in PES; the shallow-energy one is at about 0.8 eV below E_F and the deep-energy one is at about 3 eV below E_F .^{24,29,38,39} This has been explained by the large peak of HI in the valence band region.^{25,28,29} T_K has been calculated by using the same HI on the basis of the impurity model.^{40,41} It is very low, about 10^{-5} K because of the small density of states near E_F . However higher T_K , about 10 K, has been

expected from the transport properties.³¹ In the present DMFT calculation, the double peak structure is obtained as was done in previous calculations. At the same time we obtained a rather higher T_K , since HI of DMFT has a sharp peak at E_F caused by the hybridization of the bands with the correlated $4f$ bands. Similar evolution of the peak at E_F in HI has been observed recently in DMFT calculation for CeP and CeAs in ref. 42. But the SO splitting and the correct exchange process through the f^2 state have not been included there. The ($j = 5/2$) Γ_7 state has a little lower energy than that of ($j = 5/2$) Γ_8 in the paramagnetic phase at $T = 300$ K as expected in experiments.

In both materials, we find that HI which is directly calculated from the $4f$ partial DOS of bands seems to be too large when we compare the calculated PES with those of experimental ones. We present the calculation using HI reduced tentatively as 0.7 of the original value.⁴⁰ It shows rather a good agreement with experimental PES.^{24,26}

In §2, we give our formulation on the basis of the LMTO method. The DES calculated by the NCA f^2v' method for the single impurity model are compared with the results of NRG in §2. Applications to Ce metal with the lattice constant of γ -Ce, and with that of α -Ce are given in §3. In §4 the calculation for CeSb is shown. Summary is given in §5. In Appendix we explained the NCA f^2v' method.

2. Formulation

2.1 LMTO-DMFT Matrix Equation

We consider the spectra of the following Hamiltonian,⁶

$$\mathcal{H} = \mathcal{H}_{\text{LDA}} + \frac{U}{2} \sum_{\mathbf{i}, \gamma} \left(\sum_{\phi^a} c_{\phi^a \mathbf{i} \Gamma \gamma}^+ c_{\phi^a \mathbf{i} \Gamma \gamma} - n_{\mathbf{i} f}^{\text{LDA}} \right)^2. \quad (1)$$

Here $c_{\phi^a \mathbf{i} \Gamma \gamma}$ is the annihilation operator for the atomic localized state, $\phi_{\mathbf{i} \Gamma \gamma}^a(\mathbf{r})$, at site \mathbf{i} with the γ orbital of the Γ irreducible representation. The quantity $n_{\mathbf{i} f}^{\text{LDA}} = \sum_{\Gamma \gamma} n_{\phi^a \mathbf{i} \Gamma \gamma}^{\text{LDA}}$ is the occupation number on the atomic $4f$ -electron per a Ce ion in the LDA calculation. We assume that the local Coulomb interaction is expressed by the $\phi_{\mathbf{i} \Gamma \gamma}^a$ orbit.

The excitation spectra are expressed by introducing the self energy terms,³

$$\mathcal{H}_{\text{DMFT}} = \mathcal{H}_{\text{LDA}} + \sum_{\mathbf{i}, (\Gamma, \gamma)} (\Sigma_{\Gamma}(\varepsilon + i\delta) + \varepsilon_{\Gamma}^a - \varepsilon_{\Gamma}^{\text{LDA}}) |\phi_{\mathbf{i} \Gamma \gamma}^a| < \phi_{\mathbf{i} \Gamma \gamma}^a |, \quad (2)$$

where ε_{Γ}^a is the single electron energy level of $4f$ state, and $\varepsilon_{\Gamma}^{\text{LDA}}$ is the energy level in the LDA calculation. The self-energy $\Sigma_{\Gamma}(\varepsilon + i\delta)$ is calculated by solving the auxiliary impurity problem in the effective medium with the use of the NCA f^2v' method,¹⁷ the outline of it is described in Appendix.

Usually, the DMFT calculation is carried out after transforming the \mathcal{H}_{LDA} part into the LCAO scheme or to the localized Wannier representation, and then using those basis functions.⁶ In this paper we include the self-energy term directly in the LMTO matrix. This simplifies the calculation because the processes of defining the localized basis function are

skipped, but instead, Greenian equation in the non-orthogonalized bases must be introduced. In later calculation we will approximate the localized $4f$ state ϕ^a by the band center orbit $\phi(-)$ which has logarithmic derivative $-\ell - 1$ on the muffin-tin surface, because it is well localized for the $4f$ state.

In the LMTO method,²⁰ the Hamiltonian \mathcal{H}_{LDA} is represented as the matrix using the LMTO bases,

$$\psi^j \mathbf{k}(\mathbf{r}) = \sum_{qL} a_{qL}^j \mathbf{k} \chi_{qL}^{\mathbf{k}}(\mathbf{r}). \quad (3)$$

Here, $a_{qL}^j \mathbf{k}$ is the expansion coefficient of the j -th eigen state with the wave number \mathbf{k} on the LMTO base of the angular momentum (ℓ, m) and spin (α) at site q in the unit cell. We denote as $L \equiv (\ell, m, \alpha)$, henceforth. The LMTO Bloch state is given as

$$\chi_{qL}^{\mathbf{k}}(\mathbf{r}) = \frac{\Phi_{qL}(-; \mathbf{r}_q)}{\sqrt{S_q/2}\Phi_{q\ell}(-)} \delta_{qq'} - \sum_{L'} \frac{\Phi_{q'L'}(+; \mathbf{r}_{q'})}{(2\ell' + 1)\sqrt{S_{q'}/2}\Phi_{q'\ell'}(+)} S_{q'L', qL}^{\mathbf{k}}, \quad (4)$$

in the sphere of q' , where $\mathbf{r}_{q'} = \mathbf{r} - \mathbf{R}_{q'}$ is the electron coordinate from the center of MT at $\mathbf{R}_{q'}$. The quantity S_q is the radius of the MT sphere, and $S_{q'L', qL}^{\mathbf{k}}$ is the structure factor.²⁰ The LMTO base function with logarithmic derivative D is given

$$\Phi_{qL}(D; \mathbf{r}) = i^\ell Y_\ell^m(\hat{\mathbf{r}}_q) \chi(\alpha) (\phi_{\nu\ell}(r_q) + \omega(D) \dot{\phi}_{\nu\ell}(r_q)), \quad (5)$$

with the omega factor $\omega(D)$ of Andersen.¹⁹ The quantity $\Phi_{qL}(-; \mathbf{r}_q)$ ($\Phi_{qL}(+; \mathbf{r}_q)$) in eq. (4) means $\Phi_{qL}(-(\ell+1); \mathbf{r}_q)$ ($\Phi_{qL}(\ell; \mathbf{r}_q)$), and $\Phi_{q\ell}(\pm)$ is $\phi_{\nu\ell}(r_q) + \omega(\pm) \dot{\phi}_{\nu\ell}(r_q)$ on the MT sphere. The wave function $\phi_{\nu\ell}(r_q)$ and its dot state, $\dot{\phi}_{\nu\ell}(r_q)$ are calculated at the energy ε_ν .

The density of states (DOS) of the excitation is obtained by solving the Greenian equation of the matrix form,

$$[z\hat{O} - \hat{\mathcal{H}}_{\text{LDA}} - \hat{\Sigma}(z)]\hat{G}(z) = \hat{I}. \quad (6)$$

The notation hat of the matrices means that they are defined on the bases of $\chi_{qL}^{\mathbf{k}}$. As noted previously, the LMTO bases are not orthogonalized with each others.²⁰ Therefore, we have the overlapping integral \hat{O} in eq. (6), whose matrix element is given as $O_{q'L', qL}^{\mathbf{k}} = (\chi_{q'L'}^{\mathbf{k}} | \chi_{qL}^{\mathbf{k}})$. The DOS on the f -state is given by

$$\rho_{\Gamma}^{(\text{band})}(\varepsilon) = -\frac{1}{\pi} \text{tr}[\hat{O}_{\Gamma} \hat{G}(\varepsilon + i\delta)]. \quad (7)$$

The projection operator is defined as

$$\hat{O}_{\Gamma} = \sum_{\mathbf{i} \gamma} |\phi_{\mathbf{i}(\Gamma\gamma)}^a > < \phi_{\mathbf{i}(\Gamma\gamma)}^a|. \quad (8)$$

The DMFT self-consistency calculation is carried out by the following way. (I) At first we solve the auxiliary impurity model with a trial HI and impurity level $\varepsilon_{\Gamma}^{(\text{imp.})}$, and calculate the DOS $\rho_{\Gamma}^{(\text{imp.})}(\varepsilon)$, then calculate the local impurity Green's function by the Cauchy integral,

$$G_{\Gamma}^{(\text{imp.})}(z) = \frac{1}{g_{\Gamma}} \int dx \frac{\rho_{\Gamma}^{(\text{imp.})}(x)}{z - x}, \quad (9)$$

where g_Γ is the degeneracy factor of the Γ symmetry state. (II) Then the electron self-energy due to the Coulomb interaction, $\Sigma_\Gamma(z)$ is calculated by the relation,

$$\Sigma_\Gamma(z) = z - \varepsilon_\Gamma^{(\text{imp.})} - G_\Gamma^{(\text{imp.})}(z)^{-1} - \Sigma_\Gamma^{(\text{h})}(z). \quad (10)$$

Here $\Sigma_\Gamma^{(\text{h})}(z)$ is the hybridization self-energy of the impurity problem, which is calculated by the Cauchy integral from the effective trial HI.⁴³ (III) By using the self-energy $\Sigma_\Gamma(z)$ in (6), the band problem is solved, and using the equation (7), the DOS of the band $\rho_\Gamma^{(\text{band})}(\varepsilon)$ is calculated. (IV) If $\rho_\Gamma^{(\text{band})}(\varepsilon)$ and $\rho_\Gamma^{(\text{imp.})}(\varepsilon)$ agree with each other within the tolerance, the calculation is stopped. (V) If both do not agree, local band Green's function, $G_\Gamma^{(\text{band})}(z)$ is calculated by the Cauchy integral, and we estimate new effective hybridization self-energy from the relation, $\Sigma_\Gamma^{(\text{h: new})}(z) = z - \varepsilon_\Gamma^{(\text{eff.})} - G_\Gamma^{(\text{band})}(z)^{-1} - \Sigma_\Gamma(z)$, where $\varepsilon_\Gamma^{(\text{eff.})}$ is the first moment of $\rho_\Gamma^{(\text{band})}(\varepsilon)$. (VI) Then new effective HI is calculated from the imaginary part of $\Sigma_\Gamma^{(\text{h: new})}(\varepsilon + i\delta)$. We return to the step (I).

We note that the spectrum intensity in the resolvent method is not usually normalized to be unity, because configurations of the $4f$ state are restricted to some important ones.¹⁴ This is overcome by introducing the normalization factor Z_Γ and the level shift $\Delta\varepsilon_\Gamma$ as

$$\Sigma_\Gamma(z) = \Delta\varepsilon_\Gamma + \tilde{\Sigma}_\Gamma(z) - (Z_\Gamma^{-1} - 1)(z - E_F), \quad (11)$$

where $1/Z_\Gamma^{-1}$ is the total integrated intensity of DES, and $\Delta\varepsilon_\Gamma$ is determined from the first moment of $\rho_\Gamma^{(\text{imp.})}(\varepsilon)$. These ensure the relation $\tilde{\Sigma}_\Gamma(z) \sim O(1/z)$ for large $|z|$, which is required from the usual Kramers-Kronig relation. This means that the eq. (9) is expressed as $G_\Gamma^{(\text{imp.})}(z) = [z - \varepsilon_\Gamma^{(\text{imp.})} - \Delta\varepsilon_\Gamma - \tilde{\Sigma}_\Gamma(z) + (Z_\Gamma^{-1} - 1)(z - E_F) - \Sigma_\Gamma^{(\text{h})}(z)]^{-1}$.

2.2 NCA f^2v' Method

Before going to the DMFT calculation, we compare briefly the solutions to the impurity problem obtained by four typical methods of resolvent technique.¹⁷ By the solid line in Fig. 1, we show the single particle spectra calculated by the NCA f^2v' method for simplified hybridization. We have assumed that: the conduction band has constant density of states between the energy region ($-D \sim D$) with $D = 5$; HI is $v^2\rho_c = 0.08$ with the hybridization matrix v and the density of states of the conduction band ρ_c ; the doubly degenerate f -states are located at $\epsilon_{f1} = -2.2$ and $\epsilon_{f2} = -1.9$; the Coulomb interaction constant between the f -electrons is $U = 6$. The temperature is set at $T = 1.723 \times 10^{-3}$. There appears the Kondo resonance peak just at the Fermi energy, and satellites on both sides of it. The satellites correspond to the shake up excitation $\epsilon_{f1} \rightarrow \epsilon_{f2}$ in the creation of hole or electron near the Fermi energy. The result obtained by usual NCA for the (f^0 - f^1) fluctuation model is given by the dashed line. The Kondo resonance peak is small because the exchange coupling through the f^2 configuration is not considered. Grossly T_K is estimated as $D e^{-\frac{1}{N_f J \rho_c}}$ with the exchange interaction constant, J . The constant $N_f J \rho_c$ is given as $N_f v^2 \rho_c / |\epsilon_f|$ in the usual NCA, where $|\epsilon_f|$ is the excitation energy of $f^1 \rightarrow f^0$. When the virtual excitation to the f^2 states is included in the

S-W transformation,¹⁶ this factor is replaced by the expression $N_f v^2 \rho_c / |\epsilon_f| + N_f v^2 \rho_c / |\epsilon_f + U|$. The quantity $|\epsilon_f + U|$ is the excitation energy of $f^1 \rightarrow f^2$. Though we usually expect the relation $|\epsilon_f| < |\epsilon_f + U|$, the second factor gives a comparable magnitude with the first term. Because the inverse of J appears in the exponential function, the small increase of J greatly increases T_K .

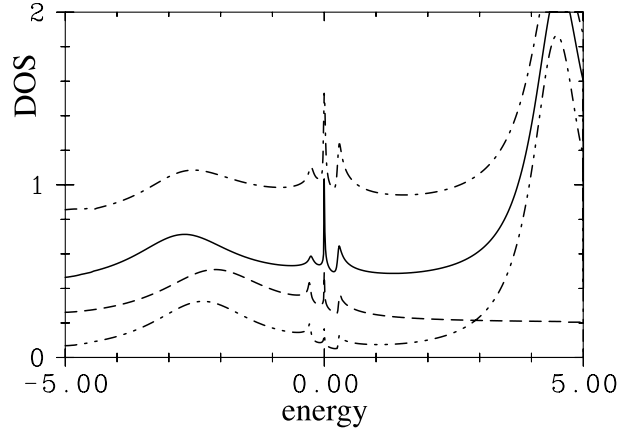


Fig. 1. Comparison of spectra calculated by several methods on the basis of the resolvent technique.

The dashed line is the result of usual NCA. The two-dots-dashed line is given by NCA type diagram including the f^2 states. The solid line is given by $\text{NCA}f^2v'$ and the dot-dashed line is given by $\text{NCA}f^2v$. Two doublets are located at $\epsilon_{f1} = -2.2$ and $\epsilon_{f2} = -1.9$. The Coulomb constant is $U = 6$ and the hybridization intensity is $v^2 \rho_c = 0.08$, the density of states of band is constant between $(-D \sim D)$ with $D = 5$. $T = 1.723 \times 10^{-3}$. The DOS of this figure is normalized as the states/spin. The zero of the lines are shifted by 0.2 successively, but the dot-dashed line by 0.4 from that of the solid line.

If we tentatively use $N_f = 2$ by assuming the energy difference $\epsilon_{f2} - \epsilon_{f1}$ to be large, T_K is estimated as $T_{K,S-W} = 7.0 \times 10^{-4}$ and $T_{K,NCA} = 5.3 \times 10^{-6}$. If we use $N_f = 4$ by assuming that the energy difference is small, T_K is estimated as $T_{K,S-W} = 0.073$ and $T_{K,NCA} = 0.0085$. These estimated values are largely different with each other. In quantitative calculations, it is important to calculate the DES by including the f^2 configuration, and also the SO and CF energy splitting.

The spectra obtained by the sum of the NCA type diagrams for the $(f^0-f^1-f^2)$ fluctuation model is given by the two-dots-dashed line. The Kondo resonance peak in this method is smaller than that of the usual (f^0-f^1) type NCA calculation. We think this result is caused by the relative decrease in f^1 state energy: the virtual excitation to the f^2 state has order $N_f - 1$ effect, and thus decreases energy in f^1 state largely; this decreases the exchange coupling of the virtual excitation to the f^0 state. On the other hand the exchange coupling through the virtual excitation to the f^2 state is not included in this approximation. Therefore

T_K decreases.

We show by the dot-dashed line the spectra calculated by a method named as $\text{NCA}f^2v$. Details of which are explained in the Appendix. In this method, the off-diagonal contribution of the vertex is added to the spectra of $\text{NCA}f^2v'$. It gives the interference effect of $f^0 \leftrightarrow f^1$ and $f^1 \leftrightarrow f^2$ processes in the final state of the single particle excited states. This effect transfers some intensity from the high excitation energy region to the low energy region, but total intensity is not changed.¹⁷ The correction is not so drastic when compared with the change from NCA to $\text{NCA}f^2v'$. The calculation of this off-diagonal correction needs the very large computing time of order N_ε^3 , while the time for diagonal part needs only N_ε^2 , where N_ε is the number of mesh points of energy. $N_\varepsilon \sim 10^5$ is needed because the width of the energy mesh should be smaller than the Kondo temperature. We use the $\text{NCA}f^2v'$ method in the DMFT band calculation in this paper.

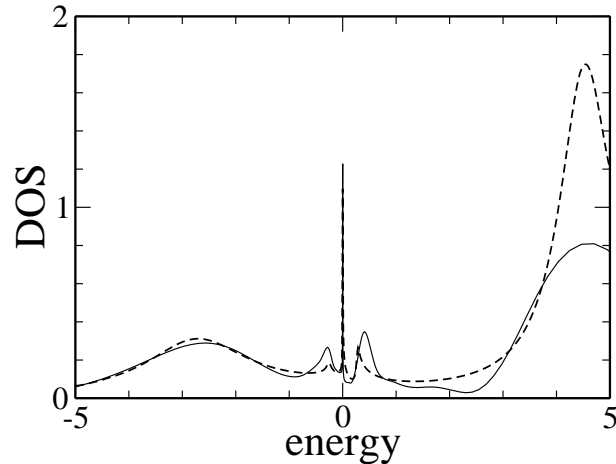


Fig. 2. Comparison of spectra calculated by $\text{NCA}f^2v'$ (dashed line) and NRG (solid line) methods. The temperatures are $T = 0.7 \times 10^{-4}$ in $\text{NCA}f^2v'$ and $T = 0$ in NRG. The parameters are the same as those in Fig. 1. The discretization parameter of NRG is $\Lambda = 2$. The peak height at the Fermi energy of $\text{NCA}f^2v'$ method is about 1.1.

In Fig. 2, we compare the spectra obtained by NRG method⁹ (solid line) at $T = 0$ and the $\text{NCA}f^2v'$ method (dashed line) at $T = 0.7 \times 10^{-4}$. This temperature is about 1/10 of the Kondo temperature, $T_{K,SW}(N_f = 2) = 7 \times 10^{-4}$, and will be low enough to compare the result of NRG at $T = 0$. The intensities of the peaks at the Fermi energy are comparable, slightly small in the $\text{NCA}f^2v'$ method. The integrated intensity of the shake up side peaks is considerably small in the $\text{NCA}f^2v'$. This points will be improved if we use the $\text{NCA}f^2v$ method, but we restrict ourselves to the $\text{NCA}f^2v'$ in this paper. We note, even the intensity of the shake up peaks is small, the present method gives the energy scale of Kondo effect not so different from the calculation of NRG. Usual NCA and $\text{NCA}f^2$ give some order of magnitude

lower Kondo temperature.

3. γ -Ce

3.1 The hybridization intensity of LDA band

As noted previously we approximate $\phi_{\mathbf{i}\Gamma\gamma}^a$ by $\phi_{\mathbf{i}\Gamma\gamma}(-)$, and $\varepsilon_\nu = \varepsilon_\Gamma^{(\text{LDA})}$ is chosen to fulfill the condition $\omega(-) = 0$. The energy $\varepsilon_\Gamma^a = \varepsilon_{4f}^a$ is changed as a parameter to lead the target of the total $4f$ occupation number. In Fig. 3, we show DOS calculated by the LDA band for the lattice constant of γ -Ce ($a = 9.75477$ AU). The $5p$ of Ce is treated as the frozen core state and the scalar relativistic approximation is used. The mesh of k -points in the band calculation is generated by taking 9 points on the $\Gamma - X$ axis (including Γ and X points). The SO interaction is added as $\zeta_\ell \mathbf{s} \cdot \ell$ in the matrix. The solid line in the top panel gives the total DOS. The shaded region in the panel gives the partial DOS on the $(j = 5/2)\Gamma_7$, the middle panel gives the partial DOS on the $(j = 5/2)\Gamma_8$, and the bottom panel gives partial DOS on the $j = 7/2$ state. The Fermi energy $E_F = 0.4585$ Ry is indicated by the vertical solid line. For the $j = 7/2$ group, DOS is summed over CF states because their splitting is not so important since they have higher excitation energy in the DMFT band. In the inset, the partial DOS's near E_F are shown for the $(j = 5/2)\Gamma_7$ (dashed line), $(j = 5/2)\Gamma_8$ (dot-dashed line) and $j = 7/2$ (dotted line) states.

The total occupation number of the $4f$ electron is obtained as 1.0859, and partial occupation numbers are shown in Table I. Hereafter we denote $\phi_{\mathbf{i}\Gamma\gamma}(-)$ as $\phi_{\mathbf{i}\Gamma\gamma}$. By using DOS $\rho_\Gamma^{(\text{LDA})}(\varepsilon)$ on the orbit $\phi_{\mathbf{i}\Gamma\gamma}$, we define Green's function $G_\Gamma^{(\text{LDA})}(z)$ by the Cauchy integral same to eq. (9). Following ref. 43, the hybridization self-energy for the non-interacting case is given as $\Sigma_\Gamma^{(\text{h,LDA})}(z) = z - \varepsilon_\Gamma^{(\text{eff,LDA})} - G_\Gamma^{(\text{LDA})}(z)^{-1}$. The HI is obtained from the imaginary part of $\Sigma_\Gamma^{(\text{h,LDA})}(\varepsilon + i\delta)$.

The HI for the LDA band is shown in Fig. 4. We note that HI of $(j = 5/2)\Gamma_7$ (upper panel) is relatively large near E_F where the $5d$ band has the large density of states, while it is small in the energy region of the deep valence band where the $6s$ band is dominant. In the inset of Fig. 3, we have shown DOS for f -components near E_F . The DOS of $(j = 5/2)\Gamma_7$ is relatively larger just below the Fermi energy than that of the $(j = 5/2)\Gamma_8$. The degeneracy factor of the state is half of the $(j = 5/2)\Gamma_8$. Therefore, HI of the $(j = 5/2)\Gamma_7$ is about twice of the $(j = 5/2)\Gamma_8$ component even when DOS has comparable value. This fact can be seen in Fig. 4. The HI of the $j = 7/2$ has the comparable magnitude with that of the $(j = 5/2)\Gamma_7$ near E_F , and with that of $(j = 5/2)\Gamma_8$ in the deep region. The averaged HI over these three groups is similar to that used in ref. 27.

When HI is strong, the f^0 -like peak in DOS of the correlated band appears below the band bottom(0.2020 Ry). In such case the peak becomes very sharp, thus it is not easy to proceed the iteration steps. To avoid such situation, we added small HI in the energy region below the band bottom in the self-consistent DMFT calculation.⁴⁵ The added part is included

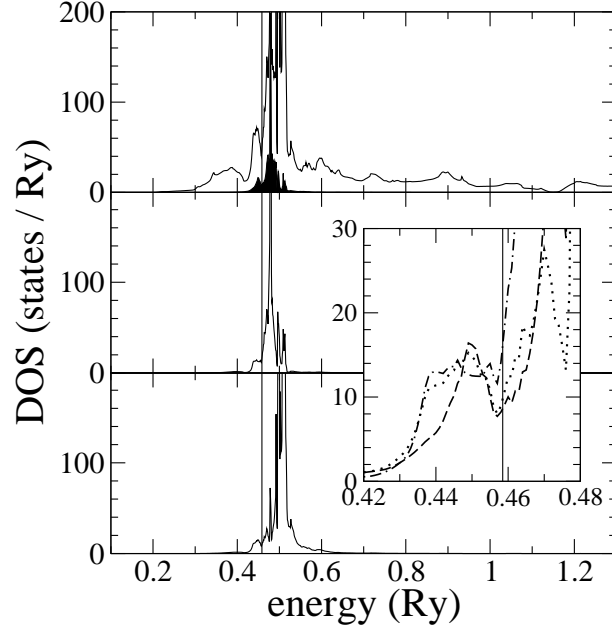


Fig. 3. The density of states (DOS) obtained by LDA band calculation for γ -Ce. The solid line in the top panel is the total DOS, the shaded region is DOS on the $(j = 5/2)\Gamma_7$, the middle panel is DOS on the $(j = 5/2)\Gamma_8$, and the bottom panel is DOS on the $j = 7/2$ states. The Fermi energy $E_F = 0.4585$ Ry is indicated by the vertical solid line. In the inset, DOS's near E_F are shown for $(j = 5/2)\Gamma_7$ (dashed line), $(j = 5/2)\Gamma_8$ (dot-dashed line) and $j = 7/2$ (dotted line) states. The standard LMTO method with ASA and CC described in ref. 20 is used. The exchange correlation function of Gunnarsson-Lundqvist⁴⁴ is employed and the lattice constant is $a = 9.75477$ AU. The frozen core approximation is used for $5p$ states.

in Fig. 4.

The $4f$ spectra calculated by using the NCA f^2v' method at $T = 300$ K for this hybridization is shown in Fig. 5. The levels are chosen to be equal to those obtained in the self-consistent calculation. The solid line gives the total $4f$ PES. The single particle DOS's for each component is also shown. Because the multiplet splitting of $4f^2$ states is neglected, we have only single large peak at about $\varepsilon_f + U \sim 0.8$ Ry for the $f^1 \rightarrow f^2$ excitation. The Coulomb interaction constant is assumed to be $U = 6.5$ eV ($= 0.48$ Ry).

The occupation numbers are shown in the row of $n_{\Gamma}^{(\text{imp}')}$ in the Table I. The occupation number of $j = 7/2$ components is reduced to 0.0959 from the value, 0.3997 of the LDA calculation. Even when the total occupation number of the $4f$ electron is not so different from the value of LDA, the partial occupation will be largely changed to the strongly correlated bands.

The relative occupation of the $(j = 5/2)\Gamma_7$ states to the $(j = 5/2)\Gamma_8$, 0.924, is large compared with 0.367 which is expected from the thermal population with their energy difference, 45K. Larger HI near E_F enhances the population of $(j = 5/2)\Gamma_7$ when the HI of the LDA

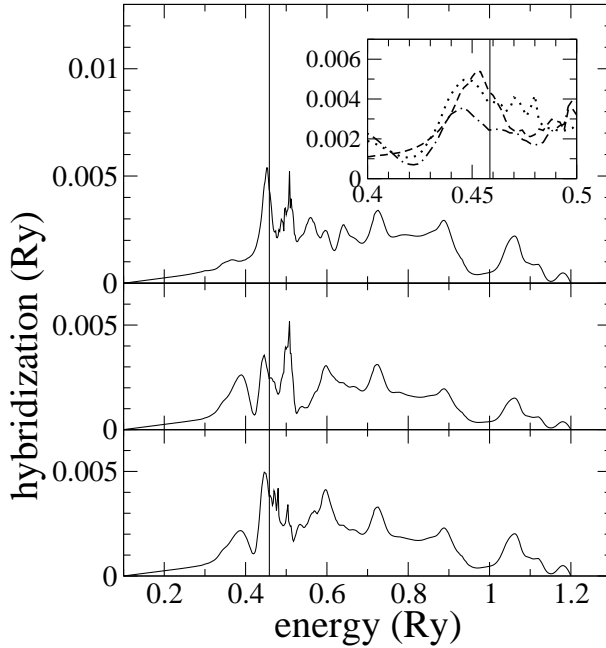


Fig. 4. Hybridization intensity (HI) calculated by the LDA band for γ -Ce. The upper panel is HI for $(j = 5/2)\Gamma_7$, the middle panel is one for $(j = 5/2)\Gamma_8$, and the lower panel is one for $j = 7/2$ state. In the inset, HI's near E_F are shown for $(j = 5/2)\Gamma_7$ (dashed line), $(j = 5/2)\Gamma_8$ (dot-dashed line) and $j = 7/2$ (dotted line) states. Small HI is added below the band bottom (at 0.2029 Ry), see the text.

band is used.

3.2 DMFT calculation

In Fig. 6, we show DOS of the $4f$ components obtained by the DMFT band calculation at $T = 300$ K.

The effective HI is shown in Fig. 7. Compared with the result in Fig. 4, the peak of HI at about 0.015 Ry below E_F is reduced. The HI in the DMFT has the small peak (or shoulder for the $j = 7/2$ component) just at E_F , and broad peaks at about 0.04 Ry above and below E_F , respectively. The HI averaged near E_F is reduced. Reflecting this the peak at E_F is relatively weak, and the SO side peak in PES becomes conspicuous in the DMFT band. Such reduction of HI just at E_F has been also observed in previous calculation.¹⁵

We started calculation by choosing the energy levels of $(j = 5/2)\Gamma_7$ and $(j = 5/2)\Gamma_8$ to be equal, -0.1500 Ry. The energy level of $j = 7/2$ is initially set as -0.1300 Ry. At the first stage, (A) HI is fixed as HI of LDA, and only energy levels are changed. We search for the solution which gives the partial occupation numbers of band with the self energy grossly agree with those of the impurity model. The target of the total occupation number of $4f$ -electron is set as 0.982. In the next stage, (B) the self-consistent spectra and the occupation numbers are determined by changing HI and levels by the iteration method. We obtain energy levels

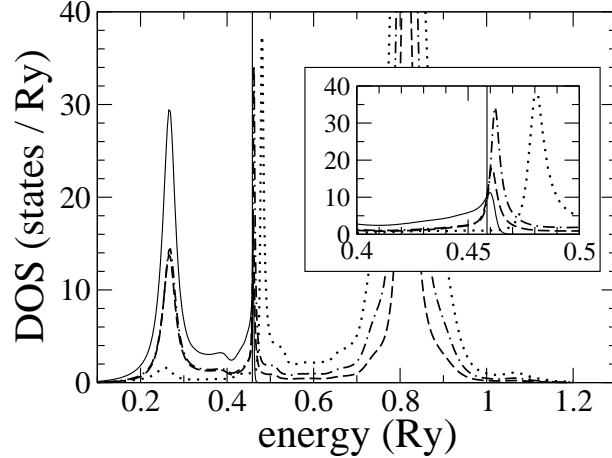


Fig. 5. $4f$ spectra calculated by using HI obtained by the LDA band for γ -Ce at $T = 300$ K. The solid line is the total $4f$ PES spectra. The dashed line is DOS of $(j = 5/2)\Gamma_7$, the dot-dashed line is DOS of $(j = 5/2)\Gamma_8$ and the dotted-line is DOS of $j = 7/2$ components. Inset shows the spectra near the Fermi energy.

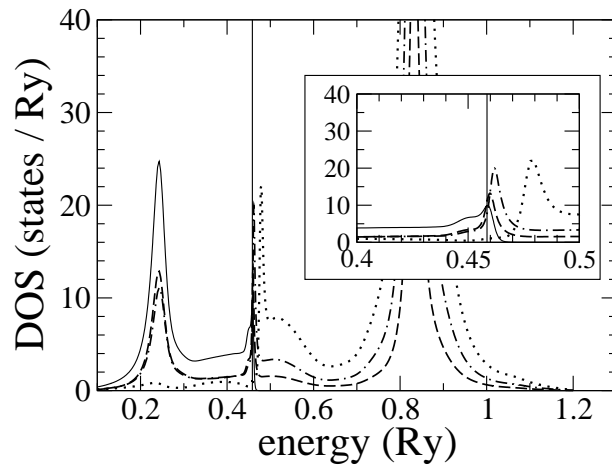


Fig. 6. $4f$ spectra of the auxiliary impurity problem for γ -Ce. For the definitions of lines, see the caption of Fig. 5.

in the auxiliary impurity model, $E((j = 5/2)\Gamma_7) = -0.14389$ Ry, $E((j = 5/2)\Gamma_8) = -0.14360$ Ry and $E(j = 7/5) = -0.12452$ Ry. Even when we skip the stage A, we can obtain similar self-consistent results, but not exactly identical ones in the strict sense because the tolerance is not small.

The occupation numbers in the auxiliary impurity problem and the DMFT band are shown in the Table I. The tolerance for the relative difference of $4f$ DOS is set to be 0.06 for the $j = 5/2$ group and 3×0.06 for the $j = 7/2$ component.

The energy level of $j = 7/2$ states is about 0.26 eV ($= -0.1245 - (-0.1439)$ Ry) higher

Table I. Various quantities obtained in DMFT calculation for γ -Ce. n_{Γ}^{LDA} is the occupation number in the LDA band, $n_{\Gamma}^{(\text{imp}')}$ is the occupation number obtained by the auxiliary impurity problem using HI of the LDA band. $n_{\Gamma}^{(\text{band})}$ is the occupation number in the DMFT band. $n_{\Gamma}^{(\text{imp.})}$ is the occupation number in the impurity problem of effective HI of DMFT calculation, ε_{Γ} is the energy level, \bar{Z}_{Γ} is the renormalization factor of the f band, and $\bar{\varepsilon}_{\Gamma}$ is the effective energy of the renormalized band. The energy levels are measured from the Fermi energy $E_F = 0.4585$ Ry, and given in Ry. The columns under $r = 1$ are the results for $r = 1$, and the columns under $r = 0.7$ are the result under the reduction factor of $r = 0.7$, see the text. The occupation numbers in columns under the $r = 0.7$ are multiplied by the factor $1/r$. $\varepsilon_{4f}^a = -0.14834$ (-0.12456)Ry for $r = 1$ ($r = 0.7$). $\zeta_{4f} = 0.007032$ Ry.

	$r = 1$			$r = 0.7$		
	Γ_7	Γ_8	$j = 7/2$	Γ_7	Γ_8	$j = 7/2$
n_{Γ}^{LDA}	0.4017	0.2845	0.3997			
$n_{\Gamma}^{(\text{imp}')}$	0.4186	0.4532	0.0959			
$n_{\Gamma}^{(\text{band})}$	0.4597	0.4153	0.1068	0.4075	0.5342	0.0415
$n_{\Gamma}^{(\text{imp.})}$	0.4604	0.4176	0.1037	0.4071	0.5342	0.0425
ε_{Γ}	-0.14389	-0.14360	-0.12452	-0.12008	-0.12012	-0.09934
\bar{Z}_{Γ}^{-1}	29.7	25.4	3.9	47.6	45.6	4.2
$\bar{\varepsilon}_{\Gamma}$	0.05304	0.14012	0.27861	0.11272	0.27732	0.43681

than the energy of $j = 5/2$. The SO splitting is slightly reduced than the value estimated by the SO constant in the LDA band calculation.

We obtained the cubic crystalline field splitting in the auxiliary impurity model, $45 \text{ K} = (-0.14360 - (-0.14389)) \text{ Ry}$, which is caused purely by the hybridization effect because we have not included the electrostatic CF field in the calculation. However, this difference should not be considered literally because the difference in HI will also cause the effective CF splitting.

In Fig. 8 we show the magnetic excitation spectra of the auxiliary impurity model, $\frac{-1}{\pi} \Im \chi(\omega) \frac{1}{1 - e^{-\beta\omega}}$, as a function of logarithm of energy (in Ry). The intensity is normalized by the value in the low energy limit. The bold solid line and the two-dots-dashed line are calculated for the effective HI for γ -Ce at $T = 300\text{K}$ (i.e., Fig. 7). The two-dots-dashed line is obtained by using the matrix element of the magnetic moment within the $j = 5/2$ manifold, while the solid line is calculated by the fictitious model in which we use the matrix within the Γ_7 manifold. The two-dots-dashed line has a peak at -2.75 , which corresponds to the excitation energy about 280 K . This peak will correspond to the excitation accompanied by the Γ_7 to Γ_8 CF transition. The solid line decreases to half of the low temperature value at -3.02 , which corresponds to the excitation energy about 150 K . This energy will be ascribed

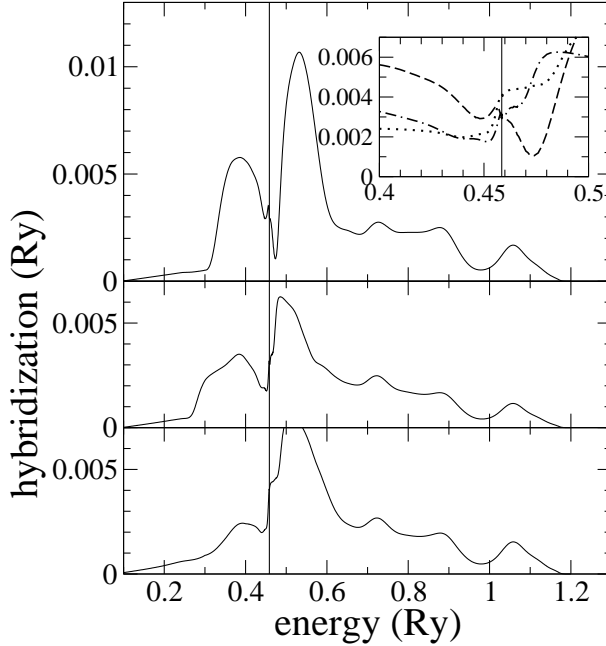


Fig. 7. Effective HI in DMFT for γ -Ce. For the definitions of lines, see the caption of Fig. 4.

to the measure of T_K in the Γ_7 state. We have also calculated the magnetic excitation for the case of Fig. 5. It decreases to half of the low energy limit at -2.6 which corresponds to 400 K. T_K is reduced in the DMFT band.

The mass renormalization factors and the effective levels are shown in the Table I. Here we have approximated as $\varepsilon_{\Gamma}^{(\text{imp.})} + \Delta\varepsilon_{\Gamma} + \tilde{\Sigma}_{\Gamma}(\varepsilon) - (Z_{\Gamma}^{-1} - 1)(\varepsilon - E_F) \sim \bar{\varepsilon}_{\Gamma} - (\bar{Z}_{\Gamma}^{-1} - 1)(\varepsilon - E_F)$. The effective levels are measured from the Fermi energy. We found that the DOS by using these parameters does not show good agreement with that obtained by the direct DMFT calculation. They give similar values only in the restricted energy region very near E_F . The renormalization factor about 30 for $j = 5/2$ states is very large. But we think these values should not be considered literally because the temperature $T = 300$ K is very high compared with the Kondo temperature. The imaginary part of the self-energy at the Fermi energy is calculated to be about 0.9 eV. The actual effect will be renormalized as $0.9/30 \sim 0.03$ eV, but is still not small.

The change of the band structure in DMFT will also be important in the quantitative calculation of the specific heat. The $4f$ component at the Fermi energy in the DMFT band (about 12 states/Ry, see the inset of Fig. 6) is small compared with that (about 35 states/Ry, see the inset of Fig. 3) in LDA. If one defines the mass enhancement factor as the ratio to the DOS of the LDA calculation, the effective factor will be reduced by the quantity, $\frac{12}{35}$.

At this point we note the difficulty in DMFT calculation. The self-energy of the hybridization is relatively very small, about 1/100 of the self-energy due to the Coulomb interaction except the energy region near E_F . The latter is roughly estimated as $Z^{-1}N_f v^2 \rho_c$ in the resol-

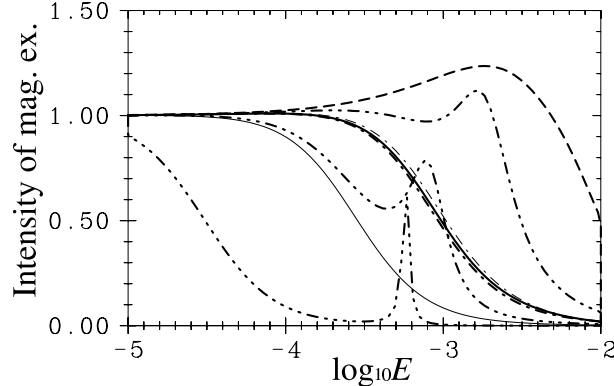


Fig. 8. Magnetic excitation spectra calculated by using the effective HI for various compounds. The bold (thin) solid line is calculated for γ -Ce with $r = 1.0(0.7)$. The bold (thin) dashed line is calculated for α -Ce with $r = 1.0(0.7)$, and the bold (thin) dot-dashed line is calculated for CeSb with $r = 1.0(0.7)$. But the thin-dashed line is not drawn because it almost overlaps on the bold solid line. The horizontal axis is the logarithm of energy in Ry, and the spectral intensities are normalized by the values at the lowest energy ($E = 10^{-7}$ Ry). For these lines, the matrix elements of magnetic moment within the Γ_7 manifold are used. Following lines are calculated by using full matrix elements in the $j = 5/2$ manifold. Two-dots-dashed line (three-dots-dashed line) is calculated for γ -Ce with $r = 1(r = 0.7)$. Four-dots-dashed line is calculated for CeSb($r = 1$) with HI of the LDA band.

vent method, and we have $Z^{-1}N_f \sim 400$, where Z^{-1} is the mass enhancement factor. This causes trouble in the iteration procedure of DMFT calculation. Usually the new trial HI is estimated from the difference of the quantities $G_{\Gamma}^{-1}(\varepsilon) = \varepsilon - \varepsilon_{\Gamma} - \Sigma_{\Gamma}^{(C)}(\varepsilon) - \Sigma_{\Gamma}^{(h)}(\varepsilon)$ obtained by the band calculation and the impurity problem for the trial HI. (In this place, the self-energy due to the Coulomb interaction is denoted as $\Sigma_{\Gamma}^{(C)}(\varepsilon)$ instead of $\Sigma_{\Gamma}(\varepsilon)$ to avoid confusion.) Usually we have relation $|\Sigma_{\Gamma}^{(C)}(\varepsilon)| \gg |\Sigma_{\Gamma}^{(h)}(\varepsilon)|$, then the very small uncertainty of $\Sigma_{\Gamma}^{(C)}(\varepsilon)$ greatly affects new trial of $\Sigma_{\Gamma}^{(h)}(\varepsilon)$, while the self-energy $\Sigma_{\Gamma}^{(C)}(\varepsilon)$ itself is very sensitive to the detail of HI. These facts lead to the unstable iteration loop. The change of the new trial HI from that of the preceding step must be restricted to be very small. Therefore, the convergence to small tolerance is very slow. The fact $|\Sigma_{\Gamma}^{(C)}(\varepsilon)| \gg |\Sigma_{\Gamma}^{(h)}(\varepsilon)|$ means, in other words, that any trial HI usually gives the almost self-consistent solution except very near E_F .

We allow the large change of HI only for the energy region near E_F .⁴⁶ We also avoid the very large number of DMFT iteration steps though the maximum relative difference of the spectral density is not so small, about 0.05 after the smoothening process of spectra.⁴⁷ Usually difference appears in the steeply increasing (or decreasing) region of the sharp peaks of the spectral density. The difference can not be reduced easily by further iteration steps. However, the difference of the peak height itself is usually small, less than about 1/10 in the relative magnitude. In addition, the large iteration loop some times leads to unphysical structure in

HI such as a superfluous gap. The tolerance for the $j = 7/2$ component is set about 3 times larger because maximum difference of it appears near the SO side peak in the unoccupied energy region not near E_F .

To give the atomic $4f$ electron number to be near unity, we obtained the $4f$ level to be about -0.144 Ry below the Fermi energy. The calculated $4f$ peak locates at about 2.7 eV below E_F , which is deep compared with the energy 2 eV observed in PES experiments.^{24,26,27} If we need the $4f$ level to appear near the experimental position, the $4f$ must be chosen to be -0.106 Ry below the Fermi energy. The occupation number of $4f$ electrons becomes about 0.90, which is very small compared with the value obtained by LDA calculation. We think that the total occupation of the $4f$ electron should not so largely change from the value of LDA, because large electrostatic energy had been already included in the LDA band.

The HI calculated on the basis of the band calculation seems to be too large. Such facts have been already noted for the impurity problem, and the reduction of the hybridization has been ascribed to the $f - d$ shielding of charge fluctuation.^{25,40} We tentatively consider the resolvent for f^0 , f^1 and f^2 states as the resolvent for f^0d^{m+1} , f^1d^m and f^2d^{m-1} states, respectively. The overlapping factor between the wave functions of d^n and $d^{n\pm 1}$ states will reduce HI. We express it by a factor $\sqrt{r}(< 1)$. The square of the hybridization, v^2 , will be reduced by r . The single particle excitation spectrum will be also reduced by the factor r because it is given by the convolution of two resolvents with different valences. We tentatively try such a simplification method.⁴⁰

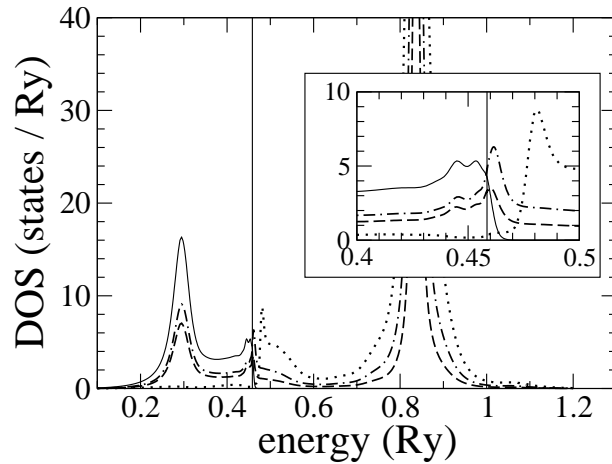


Fig. 9. $4f$ spectra calculated by reduced HI ($r = 0.7$) for γ -Ce. For the definition of r , see the text. For the definitions of lines, see the caption of Fig. 5.

In Fig. 9, we show the spectra obtained by the DMFT calculation for $r = 0.7$. The calculated result shows similar line shape given in ref. 27. The agreement with the PES experiments is improved. The obtained energy levels and the occupation numbers are shown

in the $r = 0.7$ column in the Table I. The CF splitting in the auxiliary impurity model is reversed in this case, but very small, 6 K. The magnetic excitation spectrum is shown by the thin solid line and the three-dots-dashed line in Fig. 8. they indicate $T_K \sim 56$ K. We found the $\Gamma_7 \rightarrow \Gamma_8$ excitation is about 158 K. In preceding DMFT calculations, a hump at E_F is obtained by QMC calculation,⁶ but the sharp structure has been smeared out because of the broadening and higher temperature calculations. The Kondo peak has not been observed in NCA calculation. In experimental studies, SO side peak similar to the result in Fig. 9 is observed in the high resolution experiments.^{24,26,27} Detailed comparison with experiments will be carried out in the near future.

4. α -Ce

Next we study the Ce metal with the lattice constant of α phase ($a = 9.16517$ AU). The total occupation number of the $4f$ electron in the LDA is still 1.053. We choose the target of the $4f$ electron number as 0.98 almost same to that of the γ phase. The obtained occupation numbers and the energy levels are summarized in Table II. The $4f$ DOS is shown in Fig. 10. The SO side band is almost not identified in PES, while the strong SO peak appears in the spectra above E_F . The energy level of ($j = 5/2$) Γ_8 in the auxiliary impurity model is 190 K ($= (-0.19913) - (-0.20036)$ Ry) lower than that of Γ_7 .

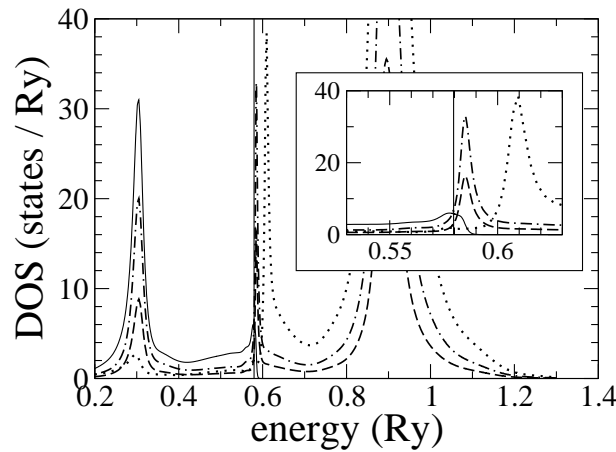


Fig. 10. $4f$ spectra of the auxiliary impurity model for α -Ce. For the definitions of lines, see the caption of Fig. 5.

The magnetic excitation spectra by using the matrix element in the Γ_7 manifold is shown by the bold dashed line in Fig. 8, which show peak at -2.7 (310 K) and decrease at -2.05 (1400 K) to half of the low energy limit. Even when we use the matrix element in the $j = 5/2$ manifold, the separated CF excitation peak does not appear in this case, but the spectrum stretches to the high energy side by 180 K.

Table II. Various quantities obtained in DMFT calculation for α -Ce. $E_F = 0.5796$ Ry, and energy levels are given in Ry. $\varepsilon_{4f}^a = -0.20423(-0.16557)$ for $r = 1$ ($r = 0.7$). $\zeta_{4f} = 0.007058$ Ry. For the definition of quantities, see the caption of Table I

	$r = 1$			$r = 0.7$		
	Γ_7	Γ_8	$j = 7/2$	Γ_7	Γ_8	$j = 7/2$
n_{Γ}^{LDA}	0.2260	0.3725	0.4545			
$n_{\Gamma}^{\text{(imp')}}_{\Gamma}$	0.4	0.4	0.0			
$n_{\Gamma}^{\text{(band)}}$	0.2515	0.5555	0.1739	0.3241	0.5862	0.0765
$n_{\Gamma}^{\text{(imp.)}}$	0.2512	0.5552	0.1745	0.3213	0.5852	0.0779
ε_{Γ}	-0.19913	-0.20036	-0.17528	-0.16002	-0.16048	-0.13790
\bar{Z}_{Γ}^{-1}	17.4	17.6	3.4	43.6	42.8	4.2
$\bar{\varepsilon}_{\Gamma}$	0.12585	0.11994	0.24659	0.17905	0.19401	0.41936

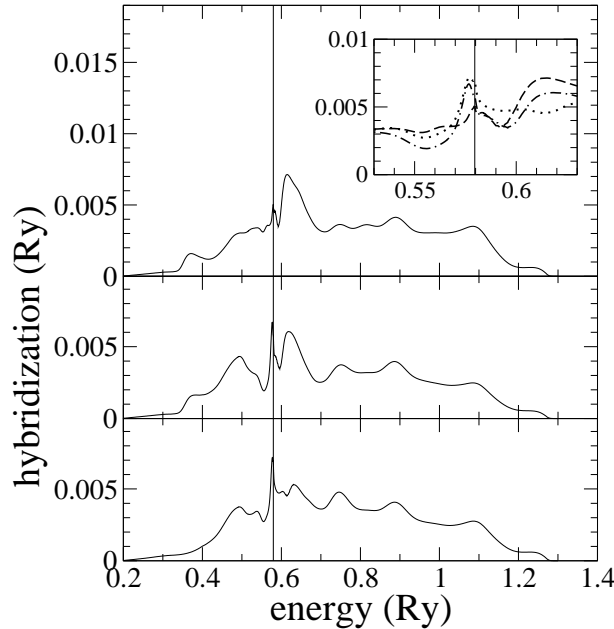


Fig. 11. Effective HI in DMFT for α -Ce. For the definitions of lines, see the caption of Fig. 4.

In Fig. 11, we show the effective HI. The HI in the energy region about 0.03 Ry below E_F is reduced, and has sharp peaks at E_F . This causes higher T_K . The renormalization factors are almost half of those in γ -Ce as seen in Table II.

In Fig. 12, we show the $4f$ DOS by using the reduction factor $r = 0.7$. The SO excitation is seen as a shoulder of the sharp peak at E_F . The energy levels and the occupation numbers are shown in the Table II. The magnetic excitation is also calculated. The spectra obtained by using the matrix element in the Γ_7 manifold overlaps on the bold solid line in Fig. 8, so we

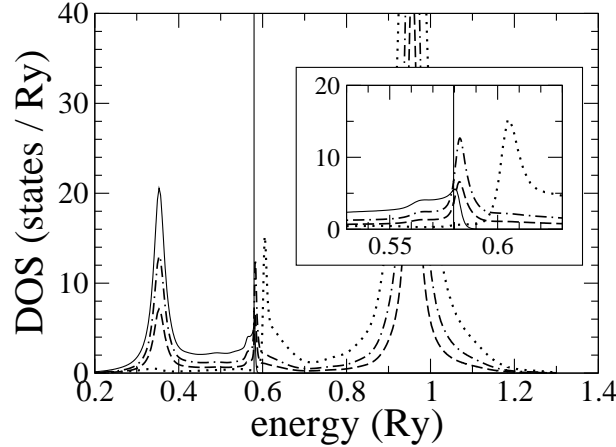


Fig. 12. $4f$ spectra calculated by reduced HI($r = 0.7$) for α -Ce. For the definition of r , see the text. For the definitions of lines, see the caption of Fig. 5.

do not have drawn there. It indicates T_K is about 160 K. Even when we use the full matrix elements in the $j = 5/2$ manifold, the separated excitation peak does not appear except a small stretch of the total spectra to the high energy side about 20K. The renormalization factors are not so different from those of γ -Ce with $r = 0.7$. The observed magnetic excitation in α -Ce has energy about 10^3 K.⁴⁹ The reduction to $r = 0.7$ seems to give a little smaller HI in α -Ce case.

5. CeSb

CeSb has NaCl structure in which Ce ions form the *fcc* lattice. The valence and the conduction bands mainly consist of the Sb $5p$ states and the Ce $5d$ states, respectively. They overlap slightly and CeSb has semi-metallic band structures. The top of the p valence band has the ($j = 3/2$) Γ_8 character, and thus has stronger hybridization matrix with the Γ_8 CF state.

In the $p - f$ mixing model, a part of the Γ_8 valence band which has the same symmetry with the occupied $4f$ band is pushed up above E_F due to the hybridization in the ordered phase.³⁰⁻³³ Such re-constructed electronic band structures in the ordered states are expected by Hatree-Fock like static mean field theory,³⁷ and confirmed by experimental studies.³⁴⁻³⁶ We need the DMFT band calculation in the paramagnetic phase.

In Fig. 13, we show the HI for CeSb of LDA band, and in Fig. 14 the effective HI of DMFT calculation. The peak of HI in the energy region $0.25 \sim 0.3$ Ry in Figs. 13 and 14 mainly corresponds to the $j = 3/2$ component of Sb p , and the peak at about 0.15 Ry corresponds to the $j = 1/2$ component.^{25,28}

In Fig. 13, we have peak structures near E_F which are caused by the hybridization of band states with the $4f$ bands. The $4f$ bands are pinned near E_F in the paramagnetic state. But

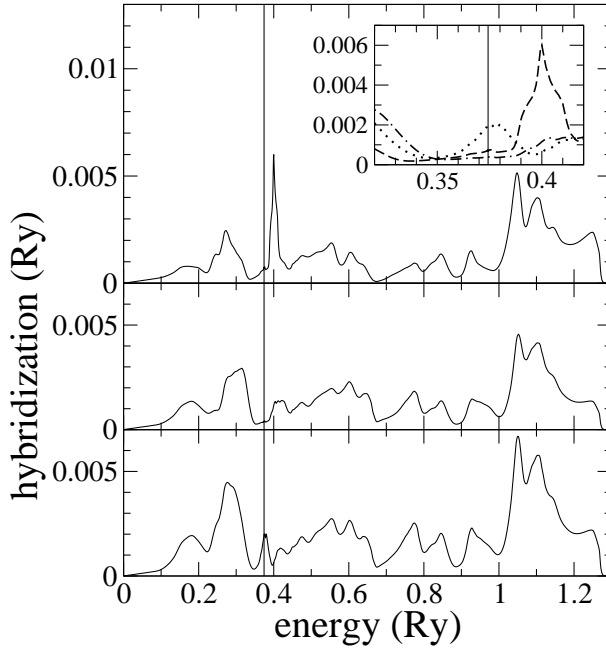


Fig. 13. The HI calculated by the LDA band for CeSb. For the definitions of lines, see the caption of Fig. 4.

the peaks do not necessarily appear just at E_F in the LDA band. We have sharp peaks just at E_F in the DMFT calculation as shown in Fig. 14. This may be caused by the hybridization with the correlated $4f$ band.

In the single particle spectra shown by Fig. 15, the shallow-energy peak appears at about 0.7 eV below E_F . The deep-energy peak appears at the energy of the valence band with $j = 1/2$ character. These results are similar to results in previous single impurity calculation.²⁵ Actually, the effective HI is grossly not different from HI used in the previous calculation.

The peak structure at E_F in HI of DMFT is very similar to that used by Takeshige to reproduce T_K of CeSb.⁴¹ It causes the sharp peak just at E_F in the spectra. From Fig. 8, T_K in the lowest Γ_7 is estimated as about 150K for this HI. Even when we include the $\Gamma_7 \rightarrow \Gamma_8$ excitation, the separated peak does not appear, but the energy at which the intensity decreases to half of the low energy limit becomes about 220K.

We also show the magnetic excitation for HI of LDA by the four-dots-dashed line in Fig. 8. The excitation energy in the lowest ($j = 5/2$) Γ_7 is estimated to be about 5K, which is very low compared to the value in DMFT calculation. The peak at about -3.3 , which corresponds to 45 K is due to the $\Gamma_7 \rightarrow \Gamma_8$ excitation. In the paramagnetic state, the energy level of Γ_7 in the auxiliary impurity model is lower, about 79 K.

In Fig. 16, we show the single particle excitation spectra for HI reduced by the factor $r = 0.7$. The deep-energy peak appears at almost same energy to that in Fig. 15, but the shallow-energy peak appears at 0.8 eV below E_F to be consistent with experiment, because

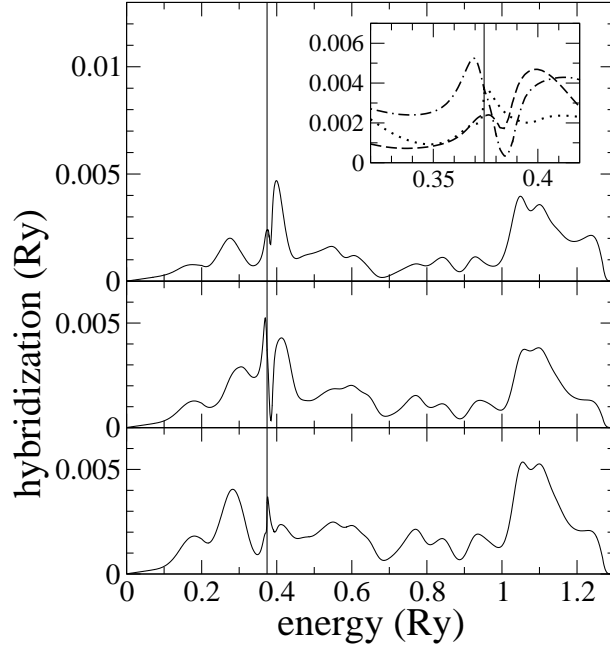


Fig. 14. Effective hybridization in DMFT for CeSb. For the definitions of lines, see the caption of Fig. 4.

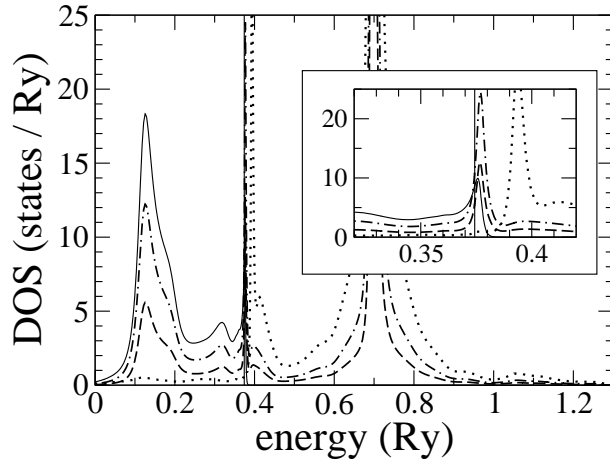


Fig. 15. $4f$ spectra of the auxiliary impurity model for CeSb. For the definitions of lines, see the caption of Fig. 5.

the level repulsion with the deep peak is reduced. We note that the height of the sharp peaks at E_F is not so different from that of Fig. 15, though HI is reduced. Actually, the magnetic excitation shows characteristic energy, about 140 K, which is not so different from that of $r = 1$ case.

The mass enhancement factors are estimated to be very large. However, these large values will not have actual meaning as already noted because we have calculated them at the high

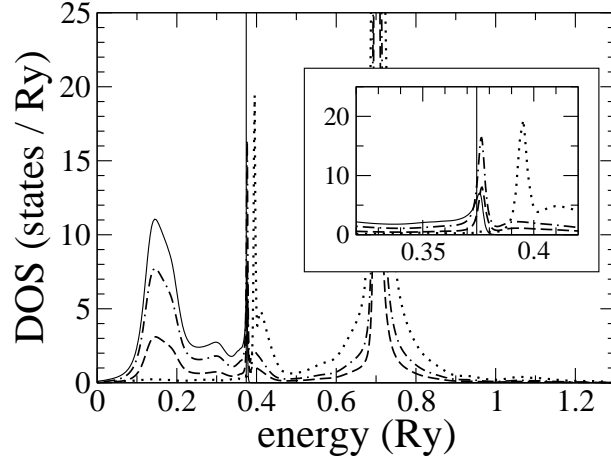


Fig. 16. $4f$ spectra calculated by reduced hybridization($r = 0.7$) for CeSb. For the definition of r , see the text. For the definitions of lines, see the caption of Fig. 5.

Table III. Various quantities obtained in DMFT calculation for CeSb. $E_F = 0.3743$ Ry, and energy levels are given in Ry. $\varepsilon_{4f}^a = -0.17242(-0.16909)$ for $r = 1$ ($r = 0.7$). $\zeta_{4f} = 0.007043$ Ry. For the definition of quantities, see the caption of Table I

	$r = 1$			$r = 0.7$		
	Γ_7	Γ_8	$j = 7/2$	Γ_7	Γ_8	$j = 7/2$
n_{Γ}^{LDA}	0.3788	0.4994	0.3178			
$n_{\Gamma}^{\text{(imp').}}$	0.3930	0.5323	0.0863			
$n_{\Gamma}^{\text{(band)}}$	0.2829	0.6276	0.0710	0.2666	0.6646	0.0538
$n_{\Gamma}^{\text{(imp.)}}$	0.2854	0.6325	0.0626	0.2682	0.6688	0.0474
ε_{Γ}	-0.17122	-0.17086	-0.15357	-0.16607	-0.16575	-0.14751
Z_{Γ}^{-1}	32.2	32.0	4.0	48.4	53.1	4.5
$\bar{\varepsilon}_{\Gamma}$	0.11174	0.10598	0.26574	0.17322	0.14272	0.38685

temperature region, $T = 300$ K. The imaginary part is calculated to be about 0.8 eV.

At this point we should note that the present calculation for CeSb has started from the LDA band. Usually it leads to rather large DOS near E_F due to the large band overlapping of Sb p and Ce d bands.⁵⁰ Very high T_K will be partly ascribed to the use of this large DOS. In transport experiments, the Kondo temperature is expected to be about 10 K.³² The correct estimation of the T_K will depend on this band overlapping. Detailed systematic studies on PES and Fermi surface structures are necessary in quantitative calculation. However, we note again, the hybridization with the correlated $4f$ band will produce sharp peaks at E_F in HI. The similar result has been also found in ref. 42. The such effect has not been considered in previous studies.²⁵ It is also necessary to analyze the transport phenomena by including the

contribution of the correlated $4f$ band.

6. Summary and Discussion

We have developed a band calculation method based on the DMFT + LMTO frame work, and applied it to Ce metal and CeSb. The starting band is calculated by the LDA method, and the auxiliary impurity problem is solved by the NCA f^2 v' method which is explained in Appendix. The method can include the f^2 configuration and gives the Kondo temperature (T_K) not the so different from that obtained by NRG, thus we can expect quantitative calculation. The spin-orbit (SO) splitting and the crystalline field (CF) splitting are included in the self-energy term. T_K is estimated from the calculation of the magnetic excitation spectra.

We studied two cases: in one case the original HI from the band is directly used ($r = 1$ case) and in another case HI is reduced to be 0.7 of its original value ($r = 0.7$ case).

In Ce metal, the total hybridization intensity (HI) near E_F is reduced in DMFT. Reflecting this the SO side peak in PES becomes relatively conspicuous compared to the calculation directly using the hybridization intensity (HI) in the LDA band. The difference of HI between ($j = 5/2$) Γ_7 and ($j = 5/2$) Γ_8 states leads to the energy level difference between them in the auxiliary impurity model. But in magnetic excitation, this difference does not directly appear because the HI itself causes the CF splitting. The estimated CF excitation energy 280K (158K) is larger than T_K 150K (56K) in γ . On the other hand CF excitation energy is smaller than T_K 1400K (160K) in α state. Here, the values in the parentheses are estimated by using the reduction factor $r = 0.7$ for HI. The calculation with the reduction factor $r = 0.7$ gives the similar result to experimental PES in γ Ce,²⁷ while $r = 0.7$ seems to give a little small HI in α Ce. In experiments the magnetic excitation in α Ce is expected to be about 10^3 K.⁴⁹ The SO splitting in DMFT calculation for Ce metal is larger than T_K , thus the Kondo temperature is greatly reduced from that estimated by calculation neglecting the SO effect. The studies of α - γ transition including the effect of SO and CF splittings are retained to the future.

For CeSb, we have obtained similar results to results of the previous calculation based on the impurity model in the gross sense. The double peak structure in PES experiments is reproduced. We have a peak very near E_F in HI. It leads to the Kondo temperature of the order of 100 K. The peak is caused by the hybridization with the correlated $4f$ band in DMFT theory. The such effect was not included in the previous impurity model. In transport experiments, the Kondo temperature is expected to be about 10 K.³¹ As noted previously, very high T_K will be partly ascribed to the large overlapping of valence and conduction bands in the LDA calculation.^{1,50} Systematic studies of band structure such as analysis of the dHvA effect,^{34,35} the angle-resolved-PES³⁹ and transport properties³¹ will be carried out in the near future.

In both materials, the HI calculated by the band calculation seems to be larger than the

magnitude expected from the comparison with PES experiment. But this may depend on the starting point of the DMFT calculation. The Coulomb interaction between $4f$ electrons is very large in atomic spectra, about 15 eV. At the same time the interaction between $4f$ and $5d$ electrons is also very large, about 10 eV. However, the effective $f - f$ Coulomb interaction is usually reduced to about $5 \sim 7$ eV in compounds. The main origin of this reduction will be ascribed to the shielding of $f - f$ interaction by the $d - f$ interaction. These points have been already noted in the calculation of the impurity model.^{25,40} We tentatively assumed that the hybridization matrix is also reduced to be about 0.7 of the original value in this the $d - f$ shielding process. This reduction leads to reasonable agreement between calculation and experimental PES. However, DMFT including the full interaction process will be necessary in the first principle calculation. This will be the future problem.

The auxiliary impurity problem is solved by the $\text{NCA}f^2v'$ method. It gives not so different excitation spectra from those calculated by NRG. However the $\text{NCA}f^2v$ gives the improved result as shown in Fig. 2. The implementation of this method will also be desirable though it will need huge computation time.

Acknowledgments

The authors would like to thank to Professor H. Shiba, Professor J. Flouquet, Professor T. Fujiwara and Dr. Ferdi Aryasetiawan for stimulation, and to Professor Y. Kuramoto for important comments on the resolvent method. The numerical computation was partly performed in the Computer Center of Tohoku University and the Supercomputer Center of Institute for Solid State Physics (University of Tokyo). This work was partly supported by JSPS and MEXT, KAKENHI(No.14340108), (No. 14540322) and (No.15034213), and the selective research fund of Tokyo Metropolitan University.

Appendix: NCA f^2v' method

Let us define the Hubbard X operator between the atomic states a and b ,

$$X(a, b) = |a><b|. \quad (\text{A}\cdot1)$$

We denote by $|0>$ the f^0 state, and by $|\eta>$ the states in which the η orbital is occupied. When the two electrons occupy the η and η' orbitals, the state is denoted as $|\eta\eta'>$. The atomic state of the $4f$ electron is expressed as

$$H_f = \sum_a E(a) X(a, a), \quad (\text{A}\cdot2)$$

where $E(a)$ is the energy of the atomic state. The creation operator of the f electron is also expressed as

$$f_\eta^+ = <\eta|f_\eta^+|0> X(\eta, 0) + \sum_{\eta'(\neq\eta)} <\eta\eta'|f_\eta^+|\eta'> X((\eta\eta'), \eta'). \quad (\text{A}\cdot3)$$

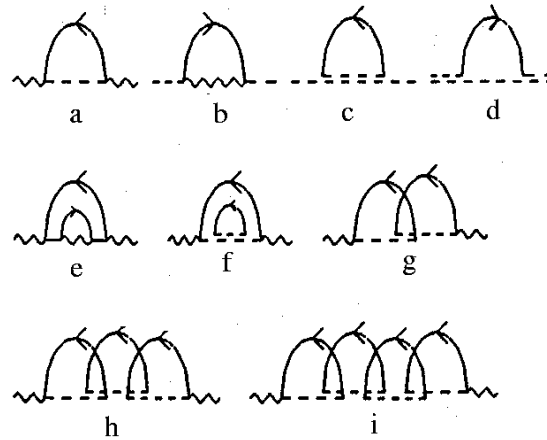


Fig. A.1. Typical diagrams in the resolvent method. top: the second order diagram for the resolvent self-energies. The wavy line denotes the f^0 resolvent, the dashed line and the double dashed line denote the f^1 and the f^2 resolvents, respectively. middle: the fourth order diagrams for the self-energy of f^0 resolvent. bottom: higher order diagrams for the f^0 resolvent, which lead to the vertex correction.

The resolvent for the atomic state a , $R(a; z)$ is expressed by using the self energy of the resolvent $\Sigma(a; z)$ as^{12,14,17}

$$R(a; z) = \frac{1}{z - E(a) - \Sigma(a; z)}. \quad (\text{A}\cdot4)$$

The skeleton diagrams of the NCA approximation which include the f^2 configuration are given in the top panel of Fig. A.1.¹⁴ The original NCA for $f^0 - f^1$ fluctuation model is given

by the diagram a and b. In the diagram a for the self-energy of the f^0 state, the fermion loop which consists of the solid and the dashed lines appears. It leads to the summation on the degeneracy factor, and has the large factor N_f . Based on this fact, the self-consistency solutions of a and b types are derived. A part of the fourth order terms for the f^0 self-energy is given in the middle panel of Fig. A·1. The diagrams e and f can be included by the skeleton diagram a of the top panel. However, the diagram g cannot be included in it. This diagram has also two loops, so it will have N_f^2 same as the g and f have. In the higher order diagrams, we must include the diagrams shown in the bottom panel of Fig. 16. Diagrams of this type for the f^0 self-energy can be summed up when we solve the integral equation for the vertex part shown graphically by top or middle panels of Fig. A·2,¹⁷

$$\Lambda(\eta; z, x) = 1 + \sum_{\eta'(\neq\eta)} \int dx' M_{\eta'}(x') R(\eta\eta'; z + x + x') R(\eta'; z + x') f(x') \Lambda(\eta'; z, x'), \quad (\text{A}\cdot5)$$

where we have used the type a equation in the Fig. A·2. The quantity $M_\eta(x)$ denotes the hybridization intensity $v^2 \rho_c(x)$.

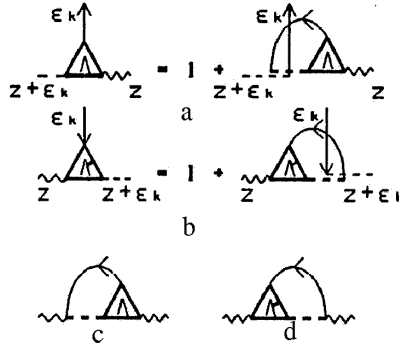


Fig. A·2. Graphical representations of the integral equation for the vertex function (top and middle panel), and the equation for the resolvent self-energy of f^0 (bottom).

The graphical expression of the f^0 self-energy is shown in the bottom panel in Fig. A·2, and the equation is given as,¹⁷

$$\Sigma(0; z) = \sum_{\eta} \int dx M_{\eta}(x) R(\eta; z + x) f(x) \Lambda(\eta; z, x). \quad (\text{A}\cdot6)$$

When one put $\Lambda(\eta; z, x) = 1$ by neglecting the contribution from the f^2 state, eq. (A·6) corresponds to the equation in the usual NCA of ($f^0 - f^1$) fluctuation.

The self-energies of the $|\eta\rangle$ state and $|\eta\eta'\rangle$ are given¹⁷

$$\begin{aligned} \Sigma(\eta; z) = & \sum_{\eta'(\neq\eta)} \int dx M_{\eta'}(x) R(\eta\eta'; z + x) f(x) \\ & + \int dx \Lambda(\eta; z - x, x) R(0; z - x) \Lambda(\eta; z - x, x) f(-x), \end{aligned} \quad (\text{A}\cdot7)$$

$$\begin{aligned}
\Sigma(\eta\eta'; z) = & \int dx (M_\eta(x)R(\eta'; z-x) + v_\eta^2 R(\eta; z-x))f(-x) \\
& + \int dx dx' M_\eta(x)M_{\eta'}(x')R(\eta'; z-x')\Lambda(\eta; z-x-x', x) \\
& \times R(0; z-x-x')\Lambda(\eta'; z-x-x', x')R(\eta; z-x)f(-x)f(-x').
\end{aligned} \tag{A.8}$$

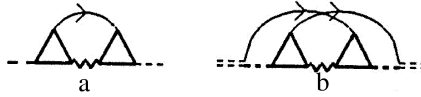


Fig. A.3. Graphical representation for the resolvent self-energies of f^1 (left panel) and f^2 (right panel) states.

The graphical expression is shown in Fig. A.3. In ref. 17, it has been pointed out that the exchange coupling due to the virtual excitation to the f^2 can be led even when the x dependence of $\Lambda(\eta; z, x)$ is neglected. The equation for the vertex is simplified as

$$\Lambda(\eta; z) = 1 + R(2)^* \sum_{\eta'(\neq\eta)} \int dx' M_{\eta'}(x')R(\eta'; z+x')f(x')\Lambda(\eta'; z). \tag{A.9}$$

where $R(2)^*$ is some representative value of the resolvent of the f^2 state for $z \sim \varepsilon_f$. We usually put as $R(2)^* = 1/(\varepsilon_f - (2\varepsilon_f + U))$. The equations (A.6) ~ (A.9) and (A.4) are solved. As discussed in ref. 17, this scheme gives the exchange constant consistent with that of the S-W transformation in the leading order of the $1/N_f$ expansion. We note that the original NCA is correct to the next order of the $1/N_f$ expansion if the valence fluctuation is restricted within $f^1 - f^0$.

The single particle excitation spectrum is given by calculating Green's function defined by

$$G_\eta = - \langle T_\tau f_\eta(\tau) f_\eta^+ \rangle. \tag{A.10}$$

By substituting eq. (A.3) into this expression, it is decomposed to Green's function defined as

$$G(ab, b'a'; \tau) = - \langle T_\tau X(ab; \tau) X(b'a') \rangle. \tag{A.11}$$

The diagonal part of the spectral function for the η particle excitation is given as the convolution integral

$$\Im G(0\eta, \eta 0 : x + i0) = \frac{1 + e^{-\beta x}}{\pi} \int dy \xi(0; y) (\Im R(\eta; y + x + i0)), \tag{A.12}$$

$$\Im G(\eta'(\eta\eta'), (\eta\eta')\eta' : x + i0) = \frac{1 + e^{-\beta x}}{\pi} \int dy \xi(\eta'; y) (\Im R(\eta\eta'; y + x + i0)), \tag{A.13}$$

where the quantities $\xi(a; x)$ is called as the defect part defined as

$$\xi(a; x) = \frac{1}{Z_f} e^{-\beta x} \left(-\frac{1}{\pi} \Im R(a; x + i0) \right). \tag{A.14}$$

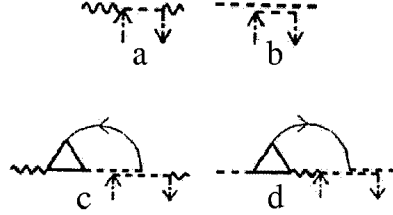


Fig. A.4. Graphical representation of the single particle excitation. The top panel is the NCA f^2v' part, and the bottom is off-diagonal part which are considered in NCA f^2v method.

The graphical expression is given by the top panel in the Fig. A.4. We note that the spectrum intensity has the off-diagonal type term shown by the bottom in the Fig. A.4, which is given as

$$\begin{aligned}
 \Im G(\eta'(\eta\eta'), \eta 0; x + i0) &= \Im G(0\eta, (\eta\eta')\eta'; x + i0) \\
 &= -\frac{1 + e^{-\beta x}}{\pi Z_f} \int dx' M_{\eta'}(x') f(-x') \int dy e^{-\beta y} \\
 &\quad \times \Im(R(\eta'; y + i0) \Lambda(\eta'; y - x' + i0) R(0; y - x' + i0)) \\
 &\quad \times \Im(R(\eta; y + x - x' + i0) R(\eta\eta'; y + x + i0)). \tag{A.15}
 \end{aligned}$$

It is known that the integration by x of (A.15) becomes zero.¹⁷ This term transfers spectral intensity in the high energy region to the low energy region. The expressions (A.12), (A.13) and (A.15) have convenient form to calculate the particle excitation part, i. e., $x > 0$. The expression can be transformed into a suitable form to calculate the hole excitation case ($x < 0$) by changing the integration variable from y to $y + x$.¹⁴

References

- 1) R. O. Jones and O. Gunnarsson: Rev. Mod. Phys. **61** (1989) 689.
- 2) Y. Kuramoto and T. Watanabe: Physica **148B** (1987) 246; W. Metzner and D. Vollhardt: Phys. Rev. Lett. **62** (1989) 324; V. Janis: Z. Phys. B **83** (1991) 227; A. Georges and G. Kotliar: Phys. Rev. B **45** (1992) 6479; F. J. Ohkawa: Phys. Rev. B **46** (1992) 9016.
- 3) A. Georges, G. Kotliar, W. Krauth, M. J. Rosenberg: Rev. Mod. Phys. **68** (1996) 13.
- 4) G. Kotliar and D. Vollhardt: Physics Today **57** (2004) 53.
- 5) A. Georges: *Proceedings of VIII Training Course in Physics of Correlated Electron Systems and High- T_C Superconductors* (American Institute of Physics) (to be published); cond-mat/0403123.
- 6) K. Held, I. A. Nekrasov, G. Keller, V. Eyert, N. Blümer, A. K. McMahan, R. T. Scalettar, T. Pruschke, V. I. Anisimov and D. Vollhardt: *Proceedings of the Winter School on “Quantum Simulations of Complex Many-Body Systems: From Theory to Algorithms”* Feb. 25-March 1 2002, Rolduc/Kerkrade(NL); cond-mat/0112079.
- 7) J. E. Gubernatis, M. Jarrell, R. N. Silver and D. S. Sivia: Phys. Rev. B **44** (1991) 6011.
- 8) M. Jarrell: Phys. Rev. Lett. **69** (1992) 168.
- 9) H. O. Frota and L. O. Oliveira: Phys. Rev. B **33** (1986) 7871; O. Sakai, Y. Shimizu and T. Kasuya: J. Phys. Soc. Jpn. **58** (1989) 3666; T. A. Costi, A. C. Hewson and V. Zlatić: J. Phys. : Condens. Matter **12** (1994) 2519.
- 10) O. Sakai and Y. Kuramoto: Solid State Commun. **89** (1994) 307. Y. Shimizu and O. Sakai: *Computational Physics as a New Frontier in Condensed Matter Research* ed. H. Takayama *et al.* (The Physical Society of Japan, Tokyo, 1994) p. 42; Y. Shimizu, O. Sakai and A. C. Hewson: J. Phys. Soc. Jpn. **69** (2000) 1777; R. Bulla, T. A. Costi and D. Vollhardt: Phys. Rev. B **64** (2001) 045103.
- 11) The QMC has limitation in application to the very strong interaction cases, and the NRG is hard to apply to cases in which the the degeneracy factor of the impurity orbital, N_f , is large.
- 12) H. Keiter and G. Morandi: Phys. Rep. **109** (1984) 227.
- 13) N. Grawe: Z. Phys. B **52** (1982) 193; Y. Kuramoto: Z. Phys. B **53** (1983) 37; H. Keiter and G. Czycholl: J. Magn. Magn. Mater. **31** (1983) 477.
- 14) N. E. Bickers: Rev. Mod. Phys. **59** (1987) 845.
- 15) M. B. Zölfli, I. A. Nekrasov, Th. Pruschke, V. I. Anisimov and J. Keller: Phys. Rev. Lett. **87** (2001) 276403-1.
- 16) J. R. Schrieffer and P. A. Wolff: Phys. Rev. **149** (1966) 491.
- 17) O. Sakai, M. Motizuki and T. Kasuya: *Core-Level Spectroscopy in Condensed Systems Theory* (Springer-Verlag, Berlin, 1988) ed. J. Kanamori and A. Kotani, p. 45.
- 18) J. Holm and K. Schönhammer: Solid State Commun. **69** (1989) 969; Th. Pruschke and N. Grawe: Z. Phys. B Condensed Matter **74** (1989) 439.
- 19) O. K. Andersen: Phys. Rev. B **12** (1975) 3060.
- 20) H. L. Skriver: *The LMTO Method* (Springer-Verlag, Berlin, 1984)
- 21) D. G. Koskenmaki and K. A. Gschneidner, Jr.: *Handbook on the Physics and Chemistry of Rare Earths*, ed. K. A. Gschneidner Jr. and L. Eyring (North-Holland, Amsterdam, 1978) p. 337.
- 22) K. Held, A. K. McMahan and R. T. Scalettar: Phys. Rev. Lett. **87** (2001) 276404-1.
- 23) A. K. McMahan, K. Held and R. T. Scalettar: Phys. Rev. B **67** (2003) 075108.
- 24) D. W. Lynch and H. Weaver: *Handbook on Physics and Chemistry of Rare-Earths*, ed. K. Gschnei-

dner, L. Eyring and S. Hüfner (North-Holland, Amsterdam, 1987) VI. 10, p.231; F. U. Hillebrecht and M. Campagna: *ibid.* p.425.

25) M. Takeshige, O. Sakai and T. Kasuya: *J. Magn. Magn. Mater.* **52** (1985) 363; M. Takeshige, O. Sakai and T. Kasuya: *Theory of Heavy Fermions and Valence Fluctuations* ed. T. Kasuya and T. Saso (Springer-Verlag, Berlin, 1985) p.120.

26) E. Weschke, C. Laubschat, T. Simmons, M. Domke, O. Strelbel and G. Kaindl: *Phys. Rev. B* **44** (1991) 8304; Yu. Kucherenko, S. L. Molodtsov, M. Heber and C. Laubschat: *Phys. Rev. B* **66** (2002) 155116; M. Grioni, P. Weibel, D. Malterre and Y. Baer: *Phys. Rev. B* **55** 2056 (1997); M. Higashiguchi, K. Shimada, T. Narimura, H. Namatame and M. Taniguchi: *Physica B* **351** 256 (2004).

27) L. Z. Liu, J. W. Allen, O. Gunnarsson, N. E. Christensen and O. K. Andersen: *Phys. Rev. B* **45** (1992) 8934.

28) O. Sakai, H. Takahashi, M. Takeshige and T. Kasuya: *Solid State Commun.* **52** (1984) 997.

29) A. Fujimori: *Phys. Rev. B* **27** (1983) 3992.

30) K. Takegahara, H. Takahashi, A. Yanase and T. Kasuya: *Solid State Commun.* **39** (1981) 857.

31) K. Kasuya, K. Takegahara, Y. Aoki, T. Suzuki, S. Kunii, M. Sera N. Sato, T. Fujita, T. Goto, A. Tamaki and T. Komatsubara: *Valence Instabilities* ed. P. Wachter and H. Boppert (1982) p. 359.

32) H. Takahashi and T. Kasuya: *J. Phys. C* **18** (1985) 2697; *ibid* 2709, 2721, 2731, 2745 and 2755.

33) F. Ishiyama and O. Sakai: *J. Phys. Soc. Jpn.* **72** (2003) 2071.

34) H. Aoki, G. W. Crabtree, W. Joss and F. Hulliger: *J. Magn. Magn. Mater.* **52** 1985 389; *J. Magn. Magn. Mater.* **97** 1991 169.

35) H. Kitazawa: *J. Magn. Magn. Mater.* **76&77** (1988) 40; R. Settai, T. Goto, S. Sakatsume, Y. S. Kwon, T. Suzuki and T. Kasuya: *J. Physica B* **186-188** (1993) 176; R. Settai, T. Goto, S. Sakatsume, Y. S. Kwon, T. Suzuki Y. Kaneta and O. Sakai: *J. Phys. Soc. Jpn.* **63** (1994) 3026; R. Settai, H. Aoki, M. Takashita, T. Terashima, Y. Haga, T. Suzuki, Y. Onuki and T. Goto: *Physica B* **216** (1996) 310.

36) R. Pittini, J. Schoenes, F. Hulliger and P. Wachter: *Phys. Rev. Lett.* **76** (1996) 3428; S. Kimura, H. Kitazawa, G. Kido and T. Suzuki: *J. Phys. Soc. Jpn.* **69** (2000) 647; S. Kimura, M. Okuno, H. Iwata, H. Kitazawa, G. Kido, F. Ishiyama and O. Sakai: *J. Phys. Soc. Jpn.* **71** (2002) 2200; S. Kimura, M. Okuno, H. Kitazawa, F. Ishiyama and O. Sakai: *J. Phys. Soc. Jpn.* **73** (2004) 2041.

37) O. Sakai, M. Takeshige, H. Harima, K. Otaki and T. Kasuya: *J. Magn. Magn. Mater.* **52** (1985) 18; O. Sakai, Y. Kaneta and T. Kasuya: *Proc. 18th Int. Conf. Low Temperature Physics* Jpn. J. Appl. Phys. **26** (1987) Suppl. 26-3; Y. Kaneta, S. Iwata, T. Kasuya and O. Sakai: *J. Phys. Soc. Jpn.* **69** (2000) 2559.

38) W. Gudat, M. Iwan, R. Pinchaux and F. Hulliger: *Valence Instabilities*, ed. P. Wachter and H. Boppert (North-Holland, Amsterdam, 1982) p. 249; D. M. Wieliczka, C. G. Olson and D. W. Lynch: *Phys. Rev. B* **29** (1984) 3028.

39) H. Kumigashira, H.-D. Kim, A. Ashihara, A. Chianani, T. Yokoya, T. Takahashi, A. Uesawa and T. Suzuki: *J. Phys. B* **56** 13654 (1997).

40) M. Takeshige, O. Sakai and T. Kasuya: *J. Phys. Soc. Jpn.* **60** (1991) 666; M. Takeshige, R. Takayama, O. Sakai and T. Kasuya: *Physical Properties of Actinide and Rare Earth Compounds* JJAP Series **8** (1993) p. 129; R. Takayama and O. Sakai: *J. Phys. Soc. Jpn.* **66** (1997) 1512.

41) M. Takeshige: Doctor Thesis for Faculty of Science, Tohoku University (1990) (unpublished).

42) J. Lægsgaard and A. Svane: Phys. Rev. B **58** 12817 (1998).

43) O. Gunnarsson, O. K. Andersen, O. Jepsen and J. Zaanen: Phys. Rev. B **39** (1989) 1708.

44) O. Gunnarsson and B. I. Lundqvist: Phys. Rev. B **13** 4274 (1976)

45) The added hybridization is given by the linear broken line: it starts at 0.1 Ry and peak at 0.3 Ry with 5×10^{-4} Ry and zero at 0.4 Ry for γ Ce. It is shifted to high energy side by 0.1 Ry in α Ce, and by -0.1 Ry in CeSb.

46) The change of trial HI from the preceding iteration step is multiplied by a factor $\frac{\Gamma^2}{(\varepsilon - E_F)^2 + \Gamma^2}$ with $\Gamma = 0.04$ Ry.

47) When we compare the spectra to check the convergence, averaging of spectra by neighboring 40 points are carried out. Because we have used logarithmic mesh near the Fermi energy, the width of the energy mesh is about 10^{-7} Ry very near the Fermi energy. The averaging process almost does not change the spectra very near the Fermi energy, but change of relative intensity about 0.1 is caused in higher energy region, $|\varepsilon - E_F| \sim 0.3$ Ry.

48) The DOS of the auxiliary impurity model with reduced HI, $r\Sigma^{(h)}(\varepsilon)$, is fitted by the expression, $G^{(imp.)}(z) = r[z - \varepsilon^{(imp.)} - \Delta\varepsilon - \Sigma - r\Sigma^{(h)}(z)]^{-1}$. This is re-written by the equation shown in the end of subsection 2.1.

49) A.P. Murani, Z. A. Bowden, A. D. Taylor, R. Osborn, and W. G. Marshall: Phys. Rev. B **48** 13981 (1993)

50) O. Sakai and Y. Kaneta: Physica B **186-188** 179 (1993).